UC Berkeley
UC Berkeley Previously Published Works

Title

Phycocyanin Fusion Constructs for Heterologous Protein Expression Accumulate as Functional Heterohexameric Complexes in Cyanobacteria

Permalink

Journal

ISSN

Authors

Martinez, Diego Hidalgo
Betterle, Nico
Melis, Anastasios

Publication Date

DOI

Peer reviewed

Phycocyanin Fusion Constructs for Heterologous Protein Expression Accumulate as Functional Heterohexameric Complexes in Cyanobacteria

Diego Hidalgo Martinez, Nico Betterle, and Anastasios Melis*

Read Online

ACCESS | Metrics & More | Article Recommendations | Supporting Information

ABSTRACT: Overexpression of heterologous proteins from plants, bacteria, and human as *fusion constructs* in cyanobacteria has been documented in the literature. Typically, the heterologous protein "P" of interest is expressed as a fusion with the abundant CpcB β-subunit of phycocyanin (PC), which was placed in the leader sequence position. The working hypothesis for such overexpressions is that CpcB*P fusion proteins somehow accumulate in a soluble and stable form in the cytosol of the cyanobacteria, retaining the activity of the trailing heterologous "P" protein of interest. The present work revealed a substantially different and previously unobvious picture, comprising the following properties of the above-mentioned CpcB*P fusion constructs: (i) the CpcB*P proteins assemble as functional $(\alpha,\beta*P)_3$CpcG heterohexameric discs, where α is the CpcA α-subunit of PC, $\beta*P$ is the CpcB*P fusion protein, the asterisk denotes fusion, and CpcG is the 28.9 kDa PC disc linker polypeptide CpcG1. (ii) The $(\alpha,\beta*P)_3$CpcG1 complexes covalently bind one open tetrapyrrole bilin co-factor per α-subunit and two bilins per β-subunit. (iii) The $(\alpha,\beta*P)_3$CpcG1 heterohexameric discs are functionally attached to the *Synechocystis* allophycocyanin (AP) core cylinders and efficiently transfer excitation energy from the assembled $(\alpha,\beta*P)_3$CpcG1 heterohexamer to the PSII reaction center, enhancing the rate of photochemical charge separation and electron transfer activity in this photosystem. (iv) In addition to the human interferon α-2 and tetanus toxin fragment C tested in this work, we have shown that enzymes such as the plant-origin isoprene synthase, β-phellandrene synthase, geranyl diphosphate synthase, and geranyl linalool synthase are also overexpressed, while retaining their catalytic activity in the respective fusion construct configuration. (v) Folding models for the $(\alpha,\beta*P)_3$CpcG1 heterohexameric discs showed the recombinant proteins P to be radially oriented with respect to the $(\alpha,\beta)_3$ compact disc. Elucidation of the fusion construct configuration and function will pave the way for the rational design of fusion constructs harboring and overexpressing multiple proteins of scientific and commercial interest.

KEYWORDS: *fusion constructs, protein overexpression, recombinant protein, Synechocystis sp. PCC 6803*
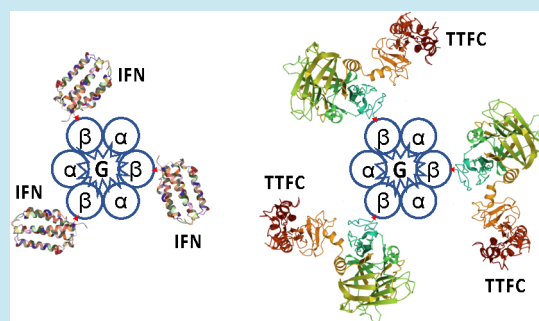
INTRODUCTION

In cyanobacteria, for example, *Synechocystis* sp. PCC 6803 (*Synechocystis*), the phycobilisomes (PBSs) comprise the major light harvesting antenna complex of photosynthesis.[1] The PBSs are composed of different proteins, which are grouped as allophycocyanin (AP) α and β subunits, phycocyanin (PC) α and β subunits, and several polypeptides acting as linker proteins.[2−5] These are organized as core AP cylinders and peripheral PC rods.[6] Covalently bound to the AP and PC proteins are bilins, open tetrapyrrole pigments that function in sunlight absorption and excitation energy transfer to the photosystem II (PSII) reaction center.[7,8] Sunlight absorbed by the PBS pigments is unidirectionally channeled from the peripheral rods, composed of PC subunit discs, to the core cylinders formed by AP subunits. The latter are found on the surface of the cyanobacterial thylakoid membranes, in close association with the membrane-bound photosystem II chlorophyll (Chl)−protein complexes. Peripheral PC rods extend

from the core cylinders into the cytoplasmic soluble phase of the cyanobacteria.[6] Substantial amino acid resources are invested by the cell to construct the sizable PBSs, comprising by far the most abundant proteins in the cell. Under nitrogen or sulfur nutrient deprivation, cyanobacteria undergo "chlorosis", comprising a well-regulated developmental program of PBS degradation to serve as a source of needed nitrogen or sulfur nutrients for survival.[9−11]

Synechocystis possesses hemispherical PBSs, whereby PC is the only biliprotein that makes up the peripheral rods. The α
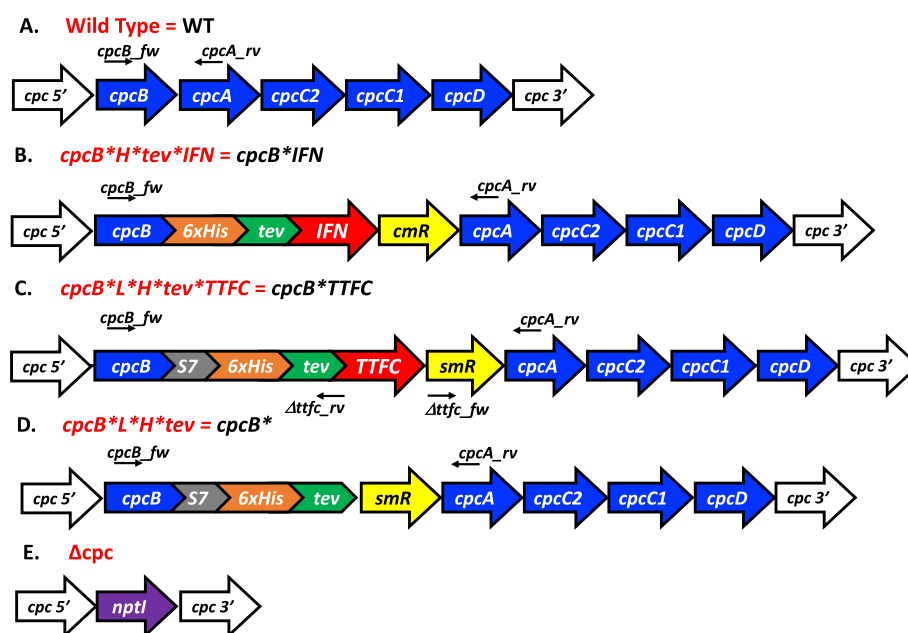
Figure 1. Schematic overview of DNA maps of the *cpc* operon in WT and *Synechocystis* transformants. (A) Native *cpc* operon, as it occurs in WT *Synechocystis*. This DNA operon configuration and sequence are referred to as the WT. (B) Replacement of the *cpcB* gene, which encodes the β-subunit of PC, with fusion construct *cpcB*6xHis*tev*IFN* harboring the interferon α-2 (IFN)-encoding DNA. This *cpcB*IFN* fusion construct was followed by the chloramphenicol (*cmR*) resistance cassette in an operon configuration. (C) Replacement of the *cpcB* gene with fusion construct *cpcB*6xHis*tev*TTFC* harboring the TTFC-encoding DNA. This *cpcB*TTFC* fusion construct was followed by the spectinomycin (*smR*) resistance cassette in an operon configuration. (D) Replacement of the *cpcB* gene with minimal fusion construct *cpcB*6xHis*tev* harboring no transgene for a heterologous protein. Such minimal *cpcB** fusion construct was followed by the spectinomycin (*smR*) resistance cassette in an operon configuration. This *cpcB** fusion was generated upon deletion of the TTFC gene from the *cpcB*6xHis*tev*TTFC* construct (C). (E) Replacement of the entire *cpc* operon native genes (*cpcB*, *cpcA*, *cpcC2*, *cpcC1*, and *cpcD*) with the kanamycin resistance cassette (*nptI*). This construct is referred to as Δ*cpc*.

(CpcA) and β (CpcB) subunits of PC dimerize into heterodimers, which then assemble into heterohexameric $(\alpha,\beta)_3$ discs that are subsequently stacked to form the peripheral rod. The PC discs that are proximal to the AP core cylinders structurally and electronically couple to the core AP through the colorless CpcG polypeptide linkers.[4,12−14] Additional colorless linker polypeptides, for example, the *cpcC1* and *cpcC2* gene products, ensure the structural stability of the middle and distal disc in the PC rods, respectively.[2−4] Since PC is the major soluble protein in cyanobacteria, the operon where it is encoded (the *cpc* operon) has been an important target for protein expression studies by several investigators.[15−19] The *cpc* operon includes, in this order, the *cpcB*, *cpcA*, *cpcC2*, *cpcC1*, and *cpcD* genes.[6]

In synthetic biology, including the generation of bioproducts in cyanobacteria, yield of the process often depends on the concentration of the pathway-catalyzing recombinant enzymes.[20,21] However, heterologous proteins are almost always unwelcomed by the host cell and either pellet as inclusion bodies or are degraded by the cell. This has been a barrier to the meaningful application of plants and microalgae in synthetic biology as it has resulted in a low steady-state level of recombinant proteins,[22−29] often much less than 0.1% of the plant tissue or alga protein content.[30] This pitfall limits carbon partitioning toward the target pathway and is negatively impacting rates and yield of product biosynthesis. Thus, true overexpression of recombinant proteins functioning in heterologous biosynthetic pathways has been a barrier and a problem in the field.

A novel CpcB*P fusion construct between the highly expressed CpcB protein in cyanobacteria and a variety of recombinant proteins "P" proved to be a suitable method for the

stable, soluble, and active recombinant enzyme overexpression in *Synechocystis*. Up to 20% of the cellular protein content, irrespective of the plant,[31,32] human,[33] or bacterial origin of the heterologous protein, was achieved.[16,34−36] This was validated with individual enzymes, including the isoprene (hemiterpene) synthase, a number of monoterpene and diterpene synthases from plants, human interferon α-2, and the bacterial isopentenyl diphosphate isomerase and tetanus toxin fragment C (TTFC), all of which were expressed to levels greater than 10% of the total cell protein.

The present work addressed the supramolecular structure, multimeric organization, and function of the CpcB*P fusion construct proteins in *Synechocystis* that enabled such hitherto unknown heterologous protein overexpression and function in these photosynthetic microorganisms.

■ RESULTS

Design of Fusion Constructs. The work is based on protein-overexpressing strains of the unicellular cyanobacterium *Synechocystis*. The focal point is the genetic engineering of the *cpc* operon, which, in the wild type (WT), encodes the light-harvesting CpcB (β-subunit) and CpcA (α-subunit) of PC and their associated CpcC2, CpcC1, and CpcD linker polypeptides. The various genetic configurations of the *cpc* operon with the heterologous genes employed in this work are shown in Figure 1. The WT *cpc* operon in *Synechocystis* is shown in Figure 1A. Fusion construct *cpcB*6xHis*tev*IFN* (abbreviated as CpcB*IFN) is the transformant whereby the human interferon α-2 encoding gene is fused to the *cpcB* gene through the six histidine and tobacco etch virus *tev* protease cleavage domain encoding DNA sequences (Figure 1B). *6xHis* was designed to
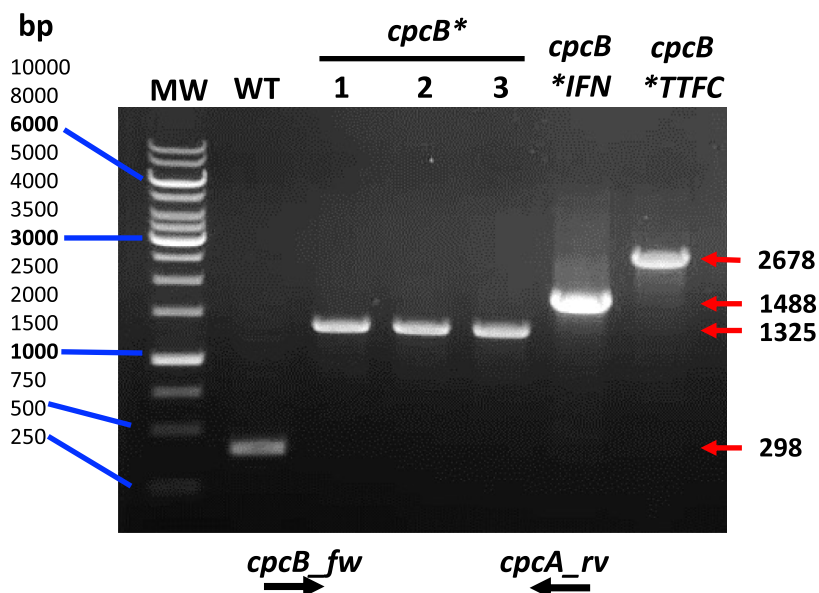
Figure 2. Genomic DNA PCR analysis testing for transgenic DNA copy homoplasmy in *Synechocystis* transformants. DNA from the WT and transformants *CpcB**, *CpcB*IFN*, and *CpcB*TTFC* was amplified using *cpcB_fw* and *cpcA_rv* primers (Figure 1). The WT yielded a 298 bp PCR product, whereas products of 1325, 1488, and 2678 bp were generated from the *cpcB**, *cpcB*IFN*, and *cpcB*TTFC* strains, respectively. Three independent *cpcB** transformant lines were tested, as this transgenic strain was not analyzed in earlier studies. Transformants *cpcB*IFN* and *cpcB*TTFC* have been tested for homoplasmy in recent studies from this lab.[33,36] Absence of 298 bp products in the transformants is evidence of DNA copy homoplasmy in these strains. Primer sequences are reported in Table S1 of the Supporting Information.
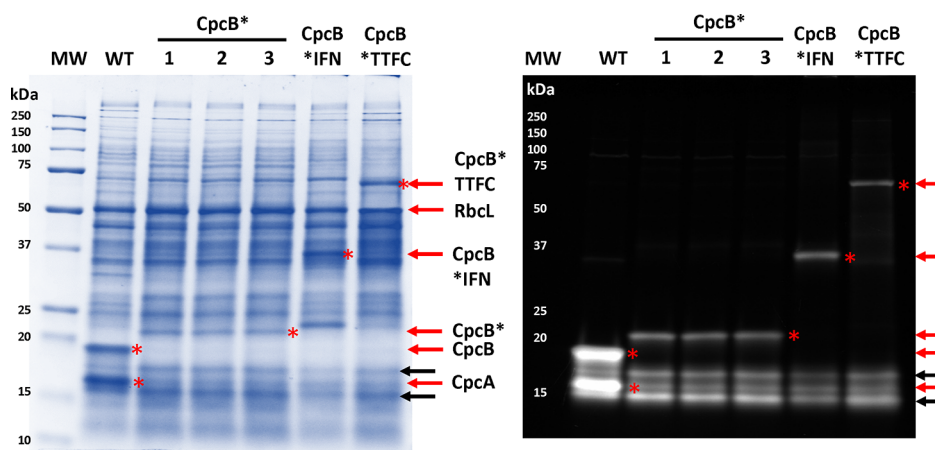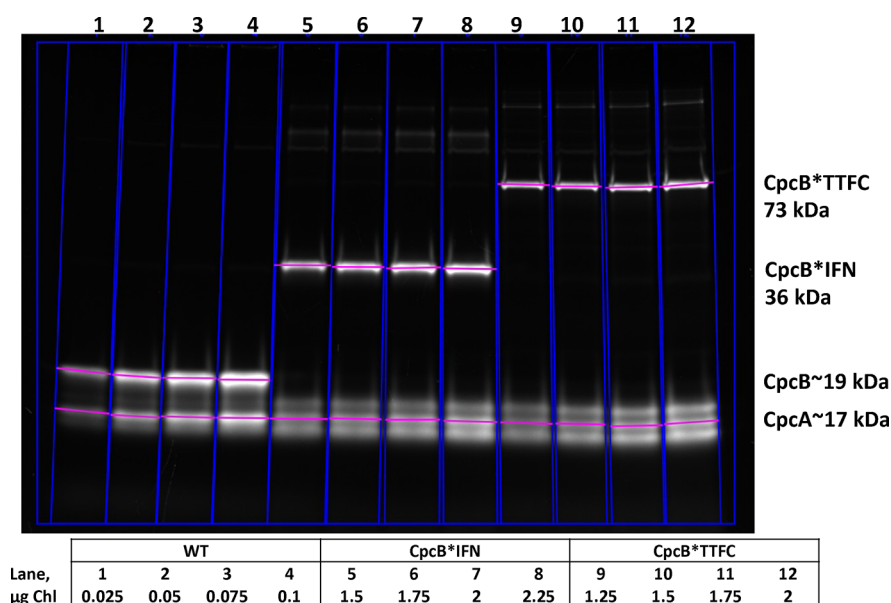

Figure 3. SDS-PAGE Coomassie staining and zinc-chromophore fluorescence of total cell extracts. The left panel shows the SDS-PAGE profile of total protein extracts stained with Coomassie. Marked by the red arrow are the PC subunits CpcA and CpcB and the CpcB*, CpcB*IFN, and CpcB*TTFC constructs (also marked by an asterisk). The right panel shows the fluorescence of the tetrapyrrole bilin pigments that are covalently bound to the AP, PC subunits CpcA and CpcB, and the CpcB*, CpcB*IFN, and CpcB*TTFC constructs (marked by red arrows). Note that CpcA Zn-chromophore fluorescence is present in the 17 kDa position, whereas all CpcB fluorescence is missing from the 19 kDa position in the CpcB*, CpcB*IFN, and CpcB*TTFC transformants. Instead, the latter showed fluorescing bands at 21, 36, and 73 kDa, respectively. The red asterisks indicate the bands that match the analysis of the SDS-PAGE Coomassie and Zn-chromophore fluorescence. Black arrows show the electrophoretic position of the core—cylinder AP proteins vs that of CpcA and CpcB in the gel.

enable isolation of the fusion protein through affinity chromatography, whereas *tev* would allow cleavage of the IFN protein from the leader CpcB*6xHis polypeptide.[36] The chloramphenicol (*cmR*) resistance cassette for transformant selection was also included in an operon configuration downstream of the fusion DNA.[33]

In a similar fashion, *cpcB*S7*6xHis*tev*TTFC* (abbreviated as CpcB*TTFC) is the transformant containing the TTFC encoding gene, followed by a spectinomycin resistance cassette (Figure 1C).[36] *S7* encodes a seven amino acid (PMPWRVI) spacer designed to change the relative orientation of CpcB and

TTFC in the fusion construct so as to enhance expression.[32] A new *cpcB*6xHis*tev* transformant (referred to as CpcB*, Figure 1D) is a variant of the CpcB*TTFC construct, and it includes only the fusion of the histidine encoding and *tev* cleavage sequences to the *cpcB* gene, followed by the spectinomycin resistance cassette. This *cpcB*6xHis*tev* (CpcB*) transformant was obtained upon removal, through site directed mutagenesis, of the coding sequence of the TTFC protein from the construct detailed in Figure 1C. Primers used for this modification were Δ*ttfc_fw* and Δ*ttfc_rv* (Figure 1C and Table S1). Lastly, the Δ*cpc* transformant is lacking the entire *cpc* operon as this was

Lane,	WT				CpcB*IFN				CpcB*TTFC			
	1	2	3	4	5	6	7	8	9	10	11	12
μg Chl	0.025	0.05	0.075	0.1	1.5	1.75	2	2.25	1.25	1.5	1.75	2

Figure 4. Zn-chromophore fluorescence profile of total cell extracts. SDS-PAGE loaded with a variable range of Chl amounts of WT (lanes 1−4), CpcB*IFN (lanes 5−8), and CpcB*TTFC (lanes 9−12). Loadings were as follows: WT (lanes 1−4): 0.025, 0.05, 0.075, and 0.1 μg of Chl. CpcB*IFN (lanes 5−8): 1.5, 1.75, 2, and 2.25 μg of Chl. CpcB*TTFC (lanes 9−12): 1.25, 1.5, 1.75, and 2 μg of Chl. The horizontal lines indicate the Zn-chromophore fluorescence bands used for the calculation of the fluorescence intensity signal and, subsequently, the CpcB/CpcA fluorescence yield ratio determination.

deleted upon replacement with the kanamycin resistance cassette (Figure 1E).[6]

Genomic DNA PCR analysis was employed to test for fusion construct locus insertion and attainment of homoplasmy in the above transformant strains. Primers *cpcB_fw* and *cpcA_rv* (Table S1) were used, overlapping the *cpcB* and *cpcA* genes, respectively (Figure 1). Results from this PCR analysis include the WT amplicon of 298 bp, CpcB* amplicon of 1325 bp, CpcB*IFN amplicon of 1488 bp, and CpcB*TTFC amplicon of 2678 bp (Figure 2). No PCR products were detected with the Δ*cpc* transformant DNA (not shown). Absence of WT products in any of the transformants examined showed complete segregation of the transformant DNA and attainment of homoplasmy in the transgenic strains.
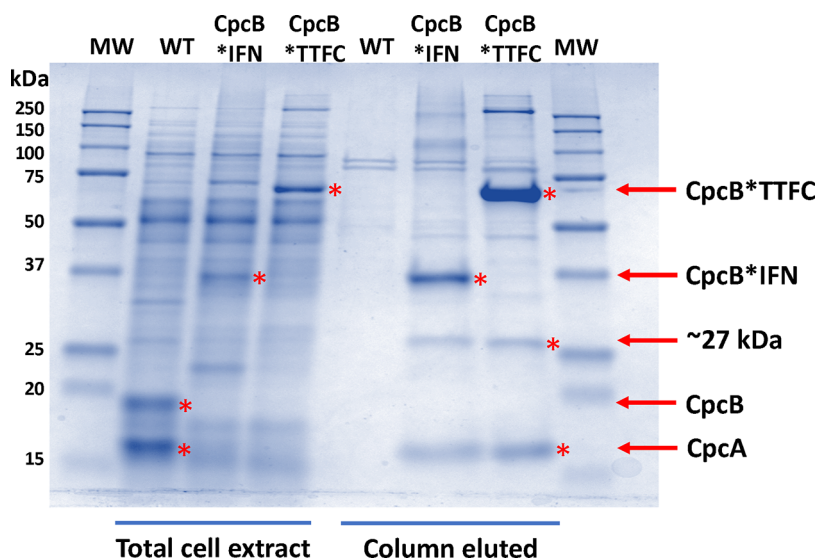
Total Cell Protein Analysis. Analysis of total cell protein extracts from the WT and transformants was undertaken via sodium dodecyl sulfate−polyacrylamide gel electrophoresis (SDS-PAGE) Coomassie stain and Zn-staining for chromophore-binding polypeptide visualization.[33] The profile of the SDS-PAGE Coomassie stain (Figure 3, WT, left panel) showed the presence of abundant CpcB (β-subunits) and CpcA (α-subunits) of PC, migrating to about 19 and 17 kDa, respectively. Also dominant is the large subunit of Rubisco (RbcL). The zinc-induced fluorescence of this SDS-PAGE protein profile, recorded using a ChemiDoc imaging system (BioRad) with UV irradiance as the light source, showed two brightly fluorescing bands at about 19 and 17 kDa (Figure 3, WT, right panel). These were attributed to the Zn-chromophore fluorescence of the CpcB and CpcA proteins, respectively.

Three independent transformant lines with the *cpcB*6xHis*-tev* (CpcB*) construct were similarly analyzed. These were devoid of the 19 kDa CpcB protein but contained substantial amounts of a ~21 kDa band, reflecting accumulation of the CpcB* protein (Figure 3, CpcB*, left panel). This assignment was supported by the results of the Zn-chromophore fluorescence analysis, showing light emission from this ~21

kDa band (Figure 3, CpcB*, right panel). The analysis of proteins from the CpcB*IFN strain showed substantial accumulation of a 36 kDa protein attributed to CpcB*6xHis*-tev*IFN, and a corresponding Zn-chromophore fluorescence band at this electrophoretic mobility position. Similarly, the analysis of proteins from the CpcB*TTFC strain showed substantial accumulation of the 73 kDa protein attributed to CpcB*6xHis*tev*TTFC, and a corresponding Zn-chromophore fluorescence band at this electrophoretic mobility position. It is of interest that all transformants showed the presence of CpcA, in amounts comparable to the level of CpcB, as visualized from the Coomassie stain (Figure 3, left panel) and Zn-chromophore fluorescence emission in the 17 kDa electrophoretic mobility position (Figure 3, right panel). Note that AP proteins also showed Zn-chromophore fluorescence emissions in the 15−18 kDa positions. However, these were distinct from the Zn-chromophore fluorescence emanating from the CpcB and CpcA proteins. These results showed the presence of some CpcA in all fusion constructs and suggested the possibility of CpcA playing a role in the stable accumulation of the CpcB*, CpcB*IFN, and CpcB*TTFC proteins. This hypothesis was investigated in greater detail.

Zn-Chromophore Quantification in Total Cell Extracts. To establish the ratio of CpcB to CpcA proteins in WT and transformant strains, a quantitative analysis of the Zn-chromophore fluorescence yield was carried out with different loadings of cell total protein extracts on multiple biological-replicate SDS-PAGE experiments, followed by Zn-chromophore fluorescence intensity analysis (Figure 4). A variable range of Chl loadings for each strain was defined to ensure an optimal signal intensity and resolution, while at the same time remaining in the linear response range for the Zn-chromophore fluorescence intensity of each band. For the WT, the range of SDS-PAGE lane loadings varied from 0.025 to 0.1 μg Chl. For the CpcB*IFN strain, a range from 1.5 to 2.25 μg Chl was optimal. For the CpcB*TTFC strain, 1.25−2 μg Chl loadings

Figure 5. Side-by-side SDS-PAGE Coomassie stain analysis of the protein profile from total *Synechocystis* cell extracts and those proteins eluted from the column affinity chromatography. The left side shows the profile of the total protein of the WT, CpcB*IFN, and CpcB*TTFC cell extracts. Marked with an asterisk are the CpcB and CpcA proteins for the WT, the 36 kDa CpcB*IFN fusion, and the 73 kDa CpcB*TTFC fusion. The right side shows the eluted fractions from the affinity column purification experiments. No WT proteins were retained/eluted from the column. The CpcB*IFN and CpcB*TTFC transformants showed the anticipated 36 and 73 kDa bands. Additionally, a ~27 kDa polypeptide and the CpcA protein were selectively and reproducibly eluted from this column chromatography.

were used. The Zn-chromophore fluorescence profile of total cell extracts from these WT, CpcB*IFN, and the CpcB*TTFC strains are shown in Figure 4. The CpcB/CpcA Zn-chromophore fluorescence yield ratio for WT, CpcB*IFN, and CpcB*TTFC were determined to be 1.51 ± 0.21, 1.41 ± 0.23, and 1.48 ± 0.31, respectively, that is, they proved to be statistically the same among the three samples in spite of the substantially different contents of the CpcB protein among the WT and transformants. The intensity of the Zn-chromophore fluorescence emission from the band below and immediately above CpcA is consistent with an assignment to components of AP of the core cylinders. Intensity of these bands in the mutants is substantially greater than that of the WT as the loading is commensurately greater in the former.

The above results were interpreted to reflect the ratio of the phycocyanobilin chromophores in the CpcB and CpcA subunits. In the PC peripheral rods, there are two phycocyanobilin molecules covalently bound to the CpcB protein and one phycocyanobilin covalently bound to CpcA.[2,3] Accordingly, a theoretical CpcB/CpcA Zn-chromophore fluorescence yield ratio of 2.0 was anticipated, at least for the WT. The lower CpcB/CpcA = 1.51 ± 0.21 Zn-chromophore fluorescence intensity ratio is probably due to a dissimilar fluorescence yield from CpcB versus that of the CpcA subunit and should be considered as such. Extrapolating this to the Zn-chromophore fluorescence ratio of the CpcB*IFN ($=1.41 \pm 0.23$) and CpcB*TTFC ($=1.48 \pm 0.31$) strains leads to the conclusion that both of these transformant strains must also contain a CpcB/CpcA phycocyanobilin ratio of 2:1, or equimolar amounts of CpcB and CpcA proteins, albeit at levels lower than those occurring in the WT.

Fusion Construct Protein Elution and Analysis. The apparently constant CpcB/CpcA phycocyanobilin ratio of 2:1 in all samples examined was investigated further upon cobalt affinity column chromatography and selective elution of the fusion proteins. This was implemented upon passing the crude cellular extracts through a His-select resin (Sigma, St. Louis,

MO, United States). Such His-tag recombinant protein binding and purification enabled elucidation of the structure and composition of a fusion construct complex, unencumbered by other cellular proteins in the SDS-PAGE analysis. A side-by-side comparison of the total cell extract and affinity chromatography column-eluted protein profiles is shown in Figure 5. Marked by the asterisk in Figure 5 (left panel) are the dominant CpcB and CpcA proteins for the WT, 36 kDa CpcB*IFN, and 73 kDa CpcB*TTFC proteins in the transformants. In the column elution experiment (Figure 5, right panel), no select proteins were eluted from the affinity column of the WT cell extracts, consistent with the absence of His-tagged recombinant proteins there. Column-eluted proteins from the CpcB*IFN and CpcB*TTFC crude extracts showed the anticipated 36 and 73 kDa constructs, respectively. They also showed the distinct presence of a protein migrating to about 27 kDa and the anticipated presence of CpcA. The amount of the ~27 kDa protein, relative to that of CpcA and CpcB was measured separately in elution experiments of proteins from the CpcB*IFN (Figure 6) and CpcB*TTFC (Figure 7) strains. Different loadings, ranging from 0.1 to 2.0 μL of the eluted sample, suggested a certain proportionality among these three eluents and possibly a structural association between the three proteins. Raw data of the scans from these (Figures 6 and 7) and similar Coomassie-stained SDS-PAGE analyses (Table S2) further raised the question of a CpcB*P/27 kDa/CpcA = 3:1:3 association as this could imitate the basic native structure of PC in the cyanobacterial peripheral rods. However, it is difficult to draw quantitative conclusions from the Coomassie stain of gels as, in some experiments, the stain level of the 27 kDa protein was lower relative to that of the CpcB*P and CpcA shown in Figures 6 and 7 (Table S2). These variations could be attributed to dissimilar rates of Coomassie staining and distaining between the CpcB*P, 27 kDa, and CpcA proteins in the various gels employed at different times during this work. (Please see the Discussion section for alternative explanations on the lower relative 27 kDa protein.) Faint protein bands migrating to ~45
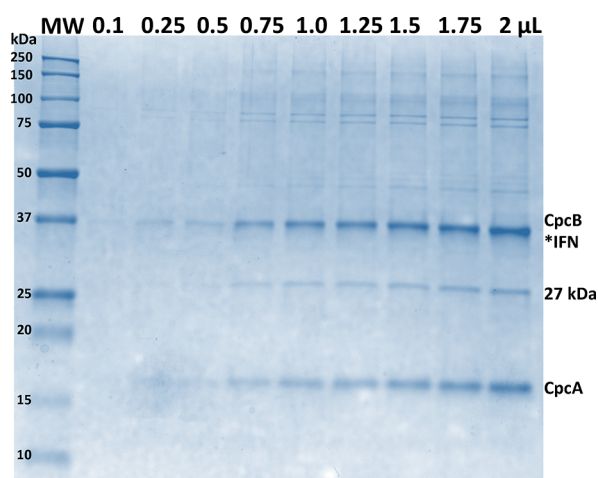
Figure 6. Quantification of proteins selectively eluted from the affinity column purification experiments of the CpcB*IFN strain. SDS-PAGE lanes were loaded with increasing volumes of the eluted fraction, shown on the top of the gel for each of the lanes. The protein profile was visualized upon staining with Coomassie brilliant blue.
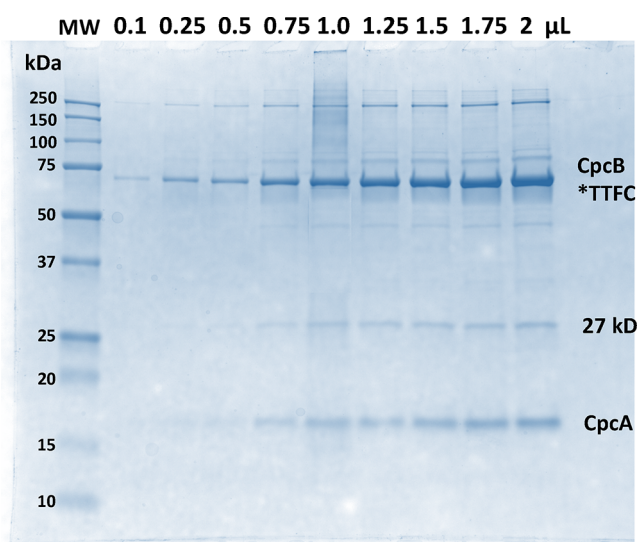
Figure 7. Quantification of proteins selectively eluted from the affinity column purification experiments of the CpcB*TTFC strain. SDS-PAGE lanes were loaded with increasing volumes of the eluted fraction, shown on the top of the gel for each of the lanes. The protein profile was visualized upon staining with Coomassie brilliant blue.

kDa could be attributed to ferredoxin NADP$^+$ oxidoreductase (FNR), traces of which are co-isolated with the fusion constructs. (Note: this FNR corresponds to the large isoform in cyanobacteria and not to the much shorter, plant-like isoform.)

The reproducible presence of the CpcB*P, 27 kDa, and CpcA proteins in column elution fractions in either the CpcB*IFN or CpcB*TTFC fusion constructs founded the hypothesis of a structural and possibly functional PC disc formation in the transformant strains, which may be responsible for the successful accumulation of such heterologous proteins, when fused to the CpcB protein. This hypothesis was investigated in greater detail.

Comparison of the Fusion Constructs and Presence of the PBS Structure. The next step comprised identification of the protein band migrating to the apparent ~27 kDa protein that was systematically eluted along with the CpcB*P fusion and CpcA proteins from the His-tag affinity column. A gel slice containing the ~27 kDa band (Figures 6 and 7) was excised from the SDS-PAGE lanes and examined using mass spectrometry (please see the Methods section). Table 1 shows the four best matching sequencing hits, where the highest probability with a 60.6% sequence coverage was for the PBS peripheral rod−core cylinder linker polypeptide CpcG1 with a calculated molecular mass of 28.9 kDa. This is the linker protein required for attachment of the peripheral PC rods to the core AP cylinders in the PBS of cyanobacteria.[2−5,13] The second best hit was the photosystem I-associated linker protein CpcG2/CpcL with a 30.5% sequence coverage. There is a close relationship between CpcG1 and CpcG2/CpcL in each of the subgroups from different cyanobacteria, where these are encountered,[5] suggesting that *cpcG1* and *cpcG2/cpcL* genes have the same origin but have apparently undergone independent divergence events during evolution, thereby explaining the sequence hit. The C-PC β-subunit was also identified as a likely hit with 27.9% sequence coverage (Table 1). The next best was the far-removed formyltetrahydrofolate deformylase as an unlikely hit with 4.9% sequence coverage. These results strongly suggest that the unknown protein migrating to ~27 kDa, as shown in Figures 5−7, is actually the 28.9 kDa *cpcG1* gene product. In addition, Table 1 reports the normalized spectral abundance factor (NSAF), which pertains to the amount of the hits measured in the samples. The NSAF for CpcG1 was greater than that for CpcG2/CpcL and also greater than those of the C-PC β-subunit and formyltetrahydrofolate deformylase. Qualitatively similar results were obtained upon consideration of the exponentially modified protein abundance index (emPAI) (not shown). These results also suggest that the unknown protein migrating to

Table 1. Mass Spectrometry Sequencing Hits of the Unknown ~27 kDa Protein Band Excised from SDS-PAGE Lanes[a]

sequence count	spectrum count	sequence coverage (%)	length	MW, dalton	NSAF	UniProt accession number
Phycobilisome Peripheral Rod−Core Cylinder Linker Polypeptide CpcG1						
31	414	60.6	249	28,902	0.896	P73093
Photosystem I-Associated Linker Protein CpcG2 or CpcL						
10	15	30.5	249	28,523	0.032	P74625
C-PC β-Subunit						
7	18	27.9	172	18,126	0.056	Q54714
Formyltetrahydrofolate Deformylase						
2	8	4.9	284	32,634	0.015	Q55135

[a]The PBS peripheral rod−core cylinder linker polypeptide CpcG1 scored the highest probability with a 60.6% sequence coverage. The NSAF, which pertains to the amount of the hits measured in the samples, also showed the CpcG1 protein to be the most abundant component of the 27 kDa excised protein band.
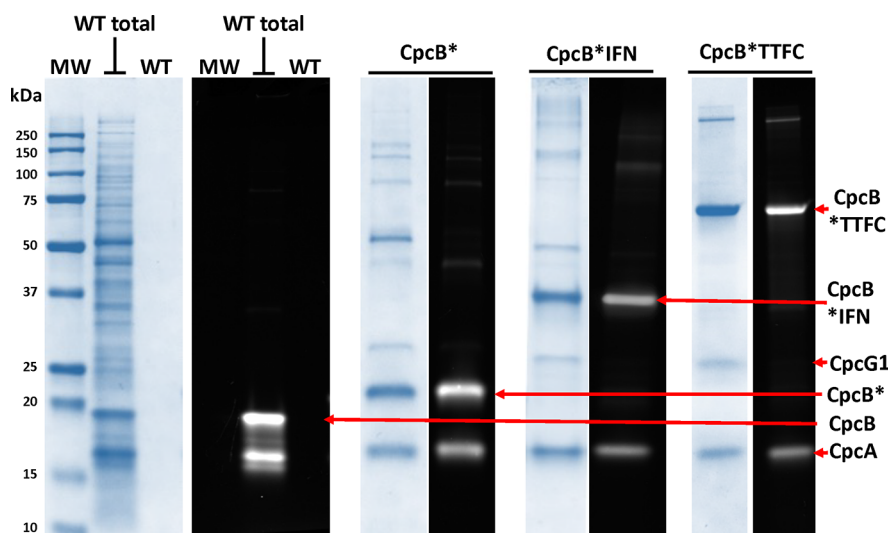
Figure 8. (Blue background panels) SDS-PAGE Coomassie stain profile of eluted protein fractions from CpcB* (21 kDa), CpcB*IFN (36 kDa), and CpcB*TTFC (73 kDa). No proteins were eluted from the affinity column purification of the WT (WT lane). A WT total protein extract (WT total, no affinity column purification) was also loaded to serve as a control. The Coomassie stains showed the presence of the CpcG1 protein in all eluted samples, migrating to about 27 kDa. (Black background panels) SDS-PAGE Zn-chromophore fluorescence of the same samples, comprising signals from the WT (WT total), CpcB* (21 kDa), CpcB*IFN (36 kDa), and CpcB*TTFC (73 kDa) proteins. (See also additional results in Figure S1.) A densitometric analysis of the Zn-chromophore fluorescence bands was carried out revealing the following intensity ratios: CpcB*/CpcA = 1.21 ± 0.12, CpcB*IFN/CpcA = 1.30 ± 0.04, and CpcB*TTFC/CpcA = 1.40 ± 0.13. The 27 kDa CpcG1 protein lacked a Zn-chromophore fluorescence emission.
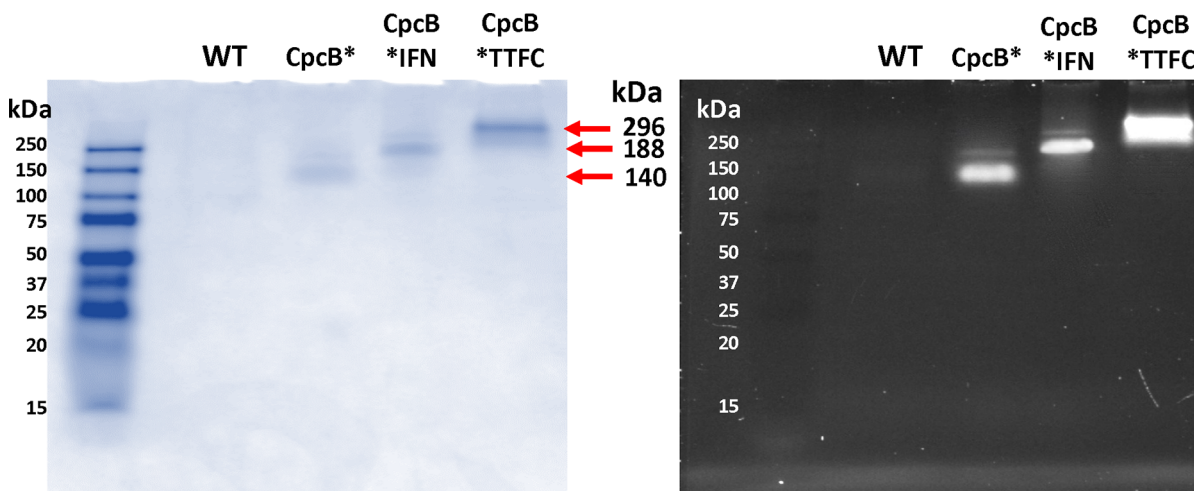
Figure 9. Native PAGE analysis of eluted proteins from the WT and the strains harboring the various CpcB*P fusion constructs. The left panel shows a Coomassie stain of the respective native PAGE analysis proteins, where a single Coomassie stained band is observed in each lane. The different electrophoretic mobilities correspond to the calculated $(\alpha,\beta^*P)_3$CpcG1 heterohexamer molecular weights of CpcB* = 140 kDa, CpcB*IFN = 188 kDa, and CpcB*TTFC = 296 kDa. The right panel shows the Zn-chromophore fluorescence profile of eluted fractions. Note that only a single Zn-chromophore fluorescence band is observed. These results suggested that the eluted fractions comprise a complex of the associated fusion and CpcG1 and CpcA proteins. 10 μL of the elution fraction was used to load each of the PAGE lanes.

~27 kDa, as shown in Figures 5−7, is actually the 28.9 kDa *cpcG1* gene product.

Zn-Chromophore Quantification in Eluted Fusion Constructs. In an effort to test for (i.e., eliminate) the possibility that the heterologous fusion protein is the reason for the CpcB*P/CpcG1/CpcA = 3:1:3 ratio allude to, the transformant of Figure 1D was used, in which the *6xHis* and *tev* DNA sequences remained fused to the *cpcB* gene but in the absence of a subsequent heterologous protein. The aim of this modification was to allow the recovery of the CpcB* protein through column purification and to find out more about the corresponding elution fraction after affinity chromatography. Results from this analysis are shown in Figure 8, where the WT

and CpcB*, CpcB*IFN, and CpcB*TTFC strains were tested. The SDS-PAGE Coomassie stain (Figure 8, blue panels) showed that no proteins were selectively eluted from the affinity chromatography of WT cell extracts. The CpcB* mutant showed a modified CpcB protein band migrating to about 21 kDa. Proteins selectively eluted from the CpcB*IFN and CpcB*TTFC samples contained the expected 36 and 73 kDa protein fusions, respectively. CpcA at 17 kDa was present in all fusion constructs, as was the CpcG1 protein. In Figure 8, black background panels show the SDS-PAGE Zn-chromophore fluorescence intensity profile of the eluted fractions associated with the above-described proteins. These elution profiles showed fluorescing bands associated with the CpcB in CpcB*,

CpcB*IFN, and CpcB*TTFC, as well as CpcA. Additional analyses of the SDS-PAGE Zn-chromophore fluorescence intensity profile of the eluted fractions, with samples in triplicate, are shown in Figure S1. Densitometric analysis was carried out to measure the CpcB/CpcA fluorescence yield ratio of the respective bands. These ratios were found to be as follows: CpcB*/CpcA = 1.21 ± 0.12/1, CpcB*IFN/CpcA = 1.30 ± 0.04/1, and CpcB*TTFC/CpcA = 1.40 ± 0.13/1. The analysis showed no statistically significant difference between the three values, consistent with the results in Figure 4, suggesting equimolar amounts of CpcB and CpcA in the eluted complexes. It may be concluded that the putative CpcB*P/CpcG1/CpcA = 3:1:3 ratio in the eluted complexes is independent and forms regardless of the presence of IFN or TTFC in the fusion constructs.

Mass Spectrometry Analysis of Eluted Proteins. Affinity chromatography eluted proteins from the transformant *Synechocystis* were subjected to mass spectrometric analysis to identify, using yet another method, protein components in the purified complexes. As a result of the total peptide sequencing analysis of these purified fractions, the same 10 proteins were identified in all eluted samples examined (results not shown). The top most significant five of these included PC components, that is, the β-subunit of PC, the α-subunit of PC, and the PBS peripheral rod−core cylinder linker polypeptide CpcG1. The other two included the AP α-chain and the ferredoxin−NADP$^+$ reductase (FNR), which appeared as a faint band below the 50 kDa marker (Figures 5−7).

Native PAGE Analysis of Fusion Construct Eluted Proteins. Selective retention during the affinity chromatography, purification, and simultaneous elution of the CpcB*P/CpcG1/CpcA proteins in a putative 3:1:3 ratio suggested that they may exist and possibly function as a coherent complex. To investigate the stoichiometry and structural association of the CpcB*P/CpcG1/CpcA proteins, a native PAGE analysis of these elutions was undertaken. Figure 9 (left panel) shows a Coomassie strain of the respective native PAGE analysis. Figure 9 (right panel) shows the corresponding Zn-chromophore fluorescence analysis. It is seen that in both analyses, no proteins were eluted from the WT, as proteins in these extracts lack the 6xHis-tag *via* which to bind to the affinity column. Results also showed that the eluted CpcB*P/CpcG1/CpcA proteins from the fusion constructs migrated as a single band in the native PAGE Coomassie and Zn-chromophore fluorescence analysis, suggesting complex formation. Figure 9 also highlights the difference in the size of the eluted complexes due to the presence of variable size heterologous fusion additions, for example, IFN or TTFC. For the CpcB* mutant without a specific recombinant protein fused (Figure 1D), the protein complex migrated to about 140 kDa, which is consistent with the calculated 140 kDa size of an $(\alpha,\beta^*)_3$CpcG1 heterohexamer. For the CpcB*IFN construct (Figure 1B), the protein complex migrated to the 190 kDa range, which is close to the calculated 188 kDa size of an $(\alpha,\beta^*IFN)_3$CpcG1 heterohexamer. Lastly, the CpcB*TTFC (Figure 1C) protein complex in Figure 9 migrated to 296 kDa, which is the estimated electrophoretic mobility of the $(\alpha,\beta^*TTFC)_3$CpcG1 heterohexamer. The 296 kDa size determination of the CpcB*TTFC complex was based on a calibration curve of the electrophoretic mobility of this complex in relation to that of the molecular weight markers shown in Figure 9 (please see the calibration curve in Figure S2). These and the preceding results show the occurrence of the structural association in the $(\alpha,\beta^*IFN)_3$CpcG1 and $(\alpha,\beta^*TTFC)_3$CpcG1

heterohexamer complexes that suggested the formation of a single PC disc, as this naturally occurs in cyanobacteria, with participation of the proximal to the core cylinder CpcG1 linker polypeptide. These results are consistent with and directly support the notion of a CpcB*P/CpcG1/CpcA=3:1:3 ratio.

Phycocyanobilin Analysis of Fusion Mutants and WT Strains. Absorbance spectra of cell suspensions were also measured to evaluate the pigment profile in the WT, *CpcB**, *CpcB*IFN*, *CpcB*TTFC*, and Δ*cpc* strains (Figure 10). The
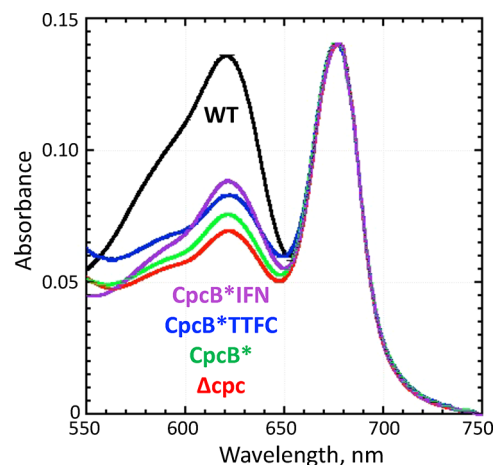
Figure 10. Absorbance spectra of the WT and CpcB*P fusion construct of intact *Synechocystis* cell suspensions. Results show the pigment profile of the WT, *CpcB**, *CpcB*IFN*, *CpcB*TTFC*, and Δ*cpc* strains. The absorbance spectra were normalized to the Chl max at 678 nm so that differences of the absorbance at 620 nm could be more readily seen among the various transformants.

absorbance spectra were normalized to the Chl max at 678 nm so that differences of the absorbance at 620 nm, where PC absorbs, could be seen among the various transformants. WT cells showed the typical absorbance bands of Chl peaking at 678 nm and PC at 620 nm. The Δ*cpc* strain (Figure 1E) lacked the entire *cpc* operon genes and, therefore, lacked the CpcB and CpcA PC proteins due to the *cpc* operon deletion.[6] The absorbance spectrum of the Δ*cpc* strain showed a low amplitude peak at 620 nm, attributed to a Chl secondary absorbance in this spectral region. The absorbance spectra of the *CpcB**, *CpcB*IFN*, and *CpcB*TTFC* cells showed a slightly elevated absorbance at 620 nm (Figure 10, see also refs 31 and 33), consistent with the presence of some phycocyanobilin chromophore in these strains. However, the amplitude of the absorbance band attributed to PC in the mutants was considerably lower than that of the WT. The ratio of PC absorbance in the transformants versus that in the WT varied in different biological replicates for the same construct and among different constructs. The average value from six independent biological replicates was measured as A(620 nm, CpcB*P)/A(620 nm, WT) = 20 ± 6.6%, that is 1:5 mutant to WT PC ratio. However, the real PC ratio is lower and closer to 1:6, as the measurement of A(620 nm, WT) is attenuated by the phenomenon of "*absorbance flattening*"[37] at 620 nm, caused by the high phycocyanobilin density in the PBSs of the WT, which is greater than that of the transformants. More specifically, WT PC rods in *Synechocystis* contain, in high density, 324 phycocyanobilin molecules, which end-up shading one another, a situation compounded by the many PBSs within each cell, as opposed to the fusion construct transformants in which a much

Table 2. Rate Constants of PSII Light Absorption and Utilization and Chl Fluorescence Yield of *Synechocystis* Transformants upon 620 nm Actinic Excitation[a]

strain	[Chl], μg mL^{-1}	12 μM DCMU, k_{II}, s^{-1}	24 μM DCMU, k_{II}-1, s^{-1}	24 μM DCMU, k_{II}-2 s^{-1}	fluorescence yield, μV signal, (normalized to Chl loaded)
Δcpc	34.0 ± 0.0	8.4 ± 0.2 (0)	8.4 ± 0.3 (0)	8.2 ± 0.6 (0)	0.0758 ± 0.002 (1.00)
CpcB*IFN	42.0 ± 4.2	11.9 ± 0.5 (3.5)	12.1 ± 1.6 (3.7)	12.6 ± 0.9 (4.4)	0.1725 ± 0.010 (1.84)
CpcB*TTFC	32.5 ± 3.5	12.2 ± 0.7 (3.8)	11.2 ± 0.4 (2.8)	11.4 ± 0.4 (3.2)	0.1201 ± 0.005 (1.66)
CpcB*	35.5 ± 0.7	13.0 ± 1.7 (4.6)	12.5 ± 1.5 (4.1)	13.7 ± 2.1 (5.5)	0.1375 ± 0.009 (1.74)
WT	32.0 ± 0.0	25.4 ± 0.8 (17.0)	25.8 ± 1.3 (17.4)	26.0 ± 0.8 (17.8)	0.230 ± 0.005 (3.03)

[a]The [Chl] column shows the Chl concentration loaded in the 1.5 mm pathlength spectrophotometer cuvette. Rates of light absorption by PSII in the Δcpc, transformants used in this work, and the WT were measured from the rate constant k_{II} of the fluorescence induction kinetics of intact cells suspended in the presence of either 12 or 24 μM DCMU. k_{II}-1 and k_{II}-2 for samples in the presence of 24 μM DCMU show the rate constants obtained upon the first illumination of dark-adapted cells (k_{II}-1), followed by a 2 min dark relaxation of the redox state of PSII and upon the second illumination and fluorescence kinetic registration of the same sample (k_{II}-2). The repeat measurement was undertaken to test for the sample and/or signal deterioration in the presence of DCMU. Numbers in parentheses show the contribution of PC to the measured k_{II}. The Chl *a* fluorescence yield was measured at 700 nm in microvolts of the photomultiplier signal output. Fluorescence yield measurements were normalized to the same [Chl] concentration and reported relative to that of the Δcpc (=1.00) sample.

lower amount of phycocyanobilin pigment is present. A differential (WT as compared to transformants) flattening correction factor of 1.26× was estimated for the WT at 620 nm. Thus, results in Figure 10 show that the mutants hold, on the average, about one-sixth the PC found in the WT.

Functional Analysis of the Heterohexameric (α,β*P)$_3$CpcG1 Complexes. The functional association of the (α,β*P)$_3$CpcG1 heterohexameric complex as a residual PC antenna in the transformants was investigated using sensitive absorbance spectrophotometry, measuring the functional PSII absorption cross-section to 620 nm light, and from the yield Φ of the Chl *a* fluorescence of intact and 3-(3,4-dichlorophenyl)-1,1-dimethylurea (DCMU)-inhibited *Synechocystis*. Cells were suspended in a 1.5 mm pathlength spectrophotometer cuvette in the range of 32−42 μg Chl mL^{-1} (Table 2). Then, weak actinic excitation at 10 μmol photons m^{-2} s^{-1} was provided at 619.5 nm by a narrow bandpass Baird Atomic interference filter coupled with a 659.6 nm visible bandpass negative cutoff Ealing filter.

The rate constant k_{II} of PSII photochemistry was measured from the fluorescence induction kinetics of intact cells suspended in the presence of either 12 or 24 μM DCMU (Table 2). Under weak 619.5 nm actinic excitation, rates of PSII photochemistry are directly proportional to the absorption cross-section at this wavelength, which depends on the number of pigment molecules acting as the antennae for this photosystem. Past studies have shown this to be a direct method for the measurement of the photosystem effective antenna size.[38,39] DCMU concentrations of 12 and 24 μM were used in these measurements with similar results. k_{II}-1 and k_{II}-2 for samples in the presence of 24 μM DCMU (Table 2) show the rate constants (rates of light absorption) obtained upon the first illumination of dark-adapted cells (k_{II}-1), followed by a 2 min dark relaxation of the redox state of PSII, and upon the second illumination and the kinetic registration of the same sample (k_{II}-2). The repeat measurement was undertaken to test for sample stability and signal reproducibility in subsequent illuminations in the presence of DCMU. It is evident that k_{II}-IFN, k_{II}-TTFC, and k_{II}-CpcB* were greater than k_{II}-Δcpc. Moreover, k_{II}-WT was substantially greater than k_{II}-Δcpc and also greater than that of the fusion construct transformants.

A quantitative assessment of these results was provided upon subtracting the contribution of the Δcpc from the k_{II} value of the transformants and from that of the WT (Table 2, k_{II} numbers in parentheses). This analysis showed that PC in the WT transfers

excitation energy to PSII 4.4 times faster than PC in the mutants (average of 17.40 vs 3.95 s^{-1}, respectively). The immediate interpretation of these results is that the WT PBS contains 4.4 times more PC than the fusion construct mutants. However, this underestimates the PBS PC pigment content in the WT by 1.26-fold because of the greater flattening of the absorbance[37] at 620 nm in the latter.

The raw Chl *a* fluorescence yield data in the microvolt signal from the apparatus and, in parentheses, the Chl *a* fluorescence yield of the various strains normalized to the same [Chl] content are reported relative to that of the Δcpc (Table 2). It is evident that all fusion transformants exhibited a greater yield of Chl *a* fluorescence. On the average, Φ(transformants) was about 1.75× greater than Φ(Δcpc). These results suggested that under these experimental conditions, higher rates of excitation energy arrived at PSII in the fusion transformants than that in the Δcpc, presumably because more actinic light was harvested (greater antenna size) in the latter than that in the Δcpc strain. Φ(WT) was 3.03× greater than Φ(Δcpc) and only about 2× greater than that of the fusion construct mutants (Table 2). However, extrapolation of these measurements to estimates of PC content in the mutant and WT strains is more tenuous in this case as the fluorescence method is indirect and there could be yield differences among the three types of strains (Δcpc, CpcB*P, and WT) employed in this work. Thus, qualitative interpretation of the fluorescence results is fine, and quantitative analysis is probably not prudent.

Taken together, the above results (Figure 10 and Table 2) are evidence that (α,β*IFN)$_3$CpcG1, (α,β*TTFC)$_3$CpcG1, and (α,β*)$_3$CpcG1 heterohexameric complexes exist in a functional association with the core AP cylinders and that they transfer excitation energy from the CpcB*P and CpcA chromophores to the PSII reaction center, thereby contributing to PSII photochemistry. A more expanded analysis is given below.

■ DISCUSSION

Overexpression of heterologous proteins as fusion constructs in cyanobacteria, with the CpcB β-subunit of PC as the leader sequence, has included divergent proteins, ranging from the isoprene synthase from kudzu,[32] the β-phellandrene synthase from a variety of plant sources,[40] the geranyl diphosphate synthase from grand fir,[20] the geranyl linalool synthase from tobacco,[41] and the human interferon α-2 protein (IFN),[33] to the bacterial TTFC.[36] The working hypothesis for such overexpressions was based on the assumption that CpcB*P fusion

proteins accumulated as soluble and stable proteins in the cytosol of the cyanobacteria, retaining the activity of the heterologous trailing moiety but preventing the assembly of the full complement of peripheral PC rods.[19,32,40,41]

The present work shows a substantially different and previously unobvious picture, comprising the following hitherto unknown properties of the above-mentioned CpcB*P fusion constructs in two alternative but not mutually exclusive models:

Model Based on the CpcB/CpcG1/CpcA = 3:1:3 Ratio.

(i) The CpcB*P proteins assemble as functional $(\alpha,\beta*P)_3G$ heterohexameric discs, where α is the CpcA α-subunit of PC, $\beta*P$ is CpcB*P fusion protein, and G is the 28.9 kDa PC linker CpcG1 polypeptide (please see below). A schematic of the minimal stable such complex is shown in Figure 11A, whereby a heterohexameric disc is made of 3CpcA α-subunits and 3CpcB β-subunits of PC. The recombinant fused proteins, depicted by the IFN and TTFC in this schematic, emanate outwardly from the heterohexameric disc, whereas the linker CpcG1 (G) protein occupies the disc center. This structure is apparently recognized by the cells as a native feature, explaining why and how the cell tolerates the presence and enables its substantial accumulation.

(ii) The CpcA α-subunits and CpcB β-subunits in the $(\alpha,\beta*P)_3G$ complex covalently bind the physiological number of open tetrapyrrole bilin chromophores, that is, one bilin per α-subunit and two bilins per β-subunit.

(iii) The $(\alpha,\beta*P)_3G$ heterohexameric disc is functionally attached to the *Synechocystis* AP core cylinders and efficiently transfers excitation energy from the assembled $(\alpha,\beta*P)_3G$ heterohexameric PC subunits to the PSII reaction center for charge separation and photochemical electron transfer (Figure 11B).

(iv) In addition to the IFN and TTFC tested in this work, proteins P in the $(\alpha,\beta*P)_3G$ heterohexameric disc have in the past been enzymes, all of which retained their catalytic activity in the respective fusion construct configurations. These observations suggested that the heterologous fusion protein P is outwardly oriented with respect to the $(\alpha,\beta)_3$ compact disc;[42] that is, it is exposed to the aqueous cytosolic medium (Figure 11A) so that it does not interfere with the anchoring of the $(\alpha,\beta*P)_3$ heterohexamer onto the *Synechocystis* AP core cylinders (Figure 11B). Accordingly, the $(\alpha,\beta*P)_3G$ heterohexameric disc performs a dual function, comprising sunlight absorption and excitation energy transfer from the α,β PC to AP and the PSII reaction center, while the fused heterologous protein P is in a position to perform its native enzymatic catalysis under in vivo conditions in the *Synechocystis* cytosol. By comparison, Figure 11C shows a schematic of the WT PBS with the native peripheral PC rods.[6] In the WT, each of the proximal (P), middle (M), and distal (D) PC discs comprise two $(\alpha,\beta)_3$ heterohexamers stacked on each other.[1–5] The dashed line in the P, M, and D discs in Figure 11C depicts the boundary between the two $(\alpha,\beta)_3$ heterohexamers. Results in this work suggest that this dimeric disc configuration is not retained in the CpcB*, CpcB*IFN, and CpcB*TTFC fusion complexes as only one $(\alpha,\beta)_3$ heterohexamer appears to be present.

(v) Pigment analysis in the fusion construct mutants showed variable amounts of PC in the transformants, estimated to
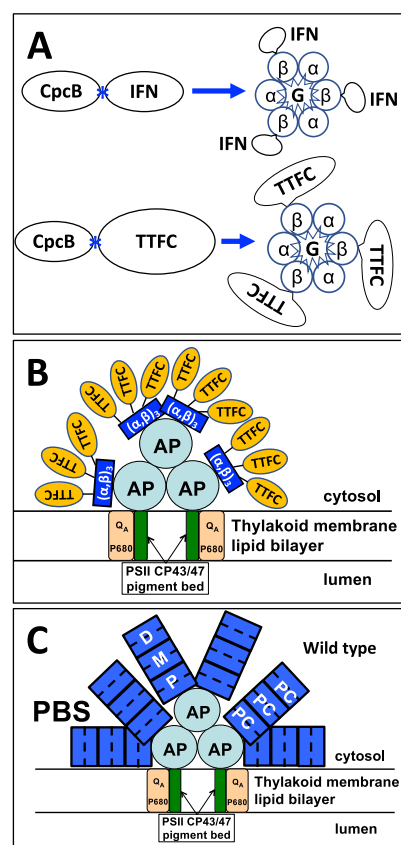
Figure 11. (A) Schematic presentation of the minimal stable $(\alpha,\beta*IFN)_3CpcG1$ and $(\alpha,\beta*TTFC)_3CpcG1$ heterohexameric complex configuration proposed in this work. IFN and TTFC are depicted as the recombinant proteins fused to the CpcB β-subunits. The CpcG1 protein (G) is proposed to occupy the disc center of the $(\alpha,\beta*IFN)_3$ and $(\alpha,\beta*TTFC)_3$ complexes. Assembly of the native α,β heterohexameric complex suggests that the corresponding heterologous fusion proteins localize away from the disc center and are likely placed at the periphery or emanate radially from the $(\alpha,\beta*IFN)_3$ and $(\alpha,\beta*TTFC)_3$ discs, thus being exposed to the medium. (B) PC configuration in the modified PBS, which is encountered in strains harboring the CpcB*P fusion protein complexes. The $(\alpha,\beta*TTFC)_3CpcG1$ heterohexameric complexes are structurally and functionally coupled to the AP core cylinders of the modified PBS so as to enable excitation energy transfer from PC to AP and then to the PSII reaction center. TTFC is depicted as the recombinant fused protein to the CpcB β-subunits in this schematic, although it could be IFN or any of the other heterologous fusion protein discussed in the literature. Note that the heterologous fusion protein is exposed to the aqueous medium in the *Synechocystis* cytosol. (C) Schematic of the WT PBS organization adapted from Kirst et al.,[6] showing the organization of the peripheral PC rods. In the WT, the proximal (P), middle (M), and distal (D) PC discs, each comprising two $(\alpha,\beta)_3$ heterohexamers, are stacked on each other. The dashed line in the P, M, and D discs depicts the separation between the two $(\alpha,\beta)_3$ heterohexamers. Results in this work suggest that this dimeric structural configuration of the PC discs is not retained in the CpcB*IFN and CpcB*TTFC fusion complexes as only one $(\alpha,\beta*P)_3$ heterohexamer is present.

be lower than 20% of that in the WT (Figure 10). This suggested a limit of one $(\alpha,\beta*P)_3G$ heterohexameric proximal disc per attachment site in the place of the peripheral PC rods in the mutants. The variable amount of PC (Figure 10), Chl fluorescence yield, and rate of photochemistry k_{II} (Table 2) noted among biologically replicate measurements suggested some variation in the

number of heterohexameric complexes occurring in association with the AP core cylinders. This variation is likely attributed to differences between cultures and growth conditions in these biological measurements.

Model Based on the CpcB/CpcG1/CPcA = 6:1:6 Ratio. It is of interest to contemplate the situation that would arise when the CpcA/CpcG1/CpcB ratio is >3:1:<3, and perhaps as high as 6:1:6, which would signify presence of two $(\alpha,\beta^*P)_3$ complexes stabilized by one CpcG1 linker. This would correspond to the in vivo structure of the full-sized proximal-to-AP PC dimer discs (Figure 11C). Our model above (Figure 11B) would be compatible with such a scenario. However, our experimental results do not seem to support large-scale accumulation of $(\alpha,\beta^*P)_3(\alpha,\beta^*P)_3G$ heterohexamer dimers. In the alternative case, when the CpcG1 protein is totally absent, the $(\alpha,\beta^*P)_3$ heterohexamers would likely not be attached to the AP core cylinders as the requisite linker is missing. It is unclear if free-floating $(\alpha,\beta^*P)_3$ heterohexamers in the cytosol can be tolerated by the cell and permitted to accumulate or if they would be degraded by the cell's proteasome.

The conclusion of the functional association of the $(\alpha,\beta^*P)_3G$ complex with the AP core cylinders received support from the observation that PC discs cannot accumulate in the cyanobacterial cell unless they are functionally associated with the AP core cylinders or the thylakoid membrane through the CpcG1 linkers.[13,36,43,44] Accordingly, key to the stability of the many CpcB*P fusion proteins examined in work from this lab is the fact that the $(\alpha,\beta^*P)_3G$ heterohexameric complexes comprise a minimal but functional light-harvesting PC discs. Otherwise, a free-floating CpcB*P fusion protein may not be stable and would be degraded due to the presence and activity of Clp proteases in the cell.[45]

The organization, functionality, and spatial arrangement of the different elements of the PBS in cyanobacteria is ensured by linker polypeptides, which provide the necessary structural support and proximity to enable light capture and efficient excitation energy transfer to the photochemical reaction center.[4–8,46–48] The proximal PC rod—AP core cylinder linkers (CpcG1) are important in the context of this work as they are primarily responsible for the structural and functional association of the peripheral PC rods, and of the $(\alpha,\beta^*P)_3G$ complex, to the AP core cylinders. In *Synechocystis*, two homologues of the *cpcG* gene exist, that is, *cpcG1* and *cpcG2*, and have been described in the literature.[13,43,44] It is most likely true that the CpcG protein in this work is the CpcG1 variant. This notion is supported both by the results in Table 1, where the "PBS peripheral rod—core cylinder linker polypeptide CpcG1" was the most abundant and presented the most hits, and by the fact that abundance and hits associated with the secondary "photosystem I-associated linker protein" were low and assigned to CpcG2 or CpcL. This notion is also consistent with results from the work by Kondo et al.,[43] who attributed a different role, for example, a state transition function to CpcG2. The consistent presence of the 28.9 kDa *cpcG1* gene product in the transformants examined in this work offers evidence that the $(\alpha,\beta^*P)_3G$ heterohexamer is the PC disc proximal to the AP core cylinders. Conversely, the absence of the 33 kDa CpcC1 and 30 kDa CpcC2 linkers supports the absence of the middle and distal PC discs in the CpcB*IFN and CpcB*TTFC fusion transformants.

The *cpcB*S*H*tev* (CpcB*) transformant containing only the *6xHis* tag and *tev* cleavage site encoding DNA (Figure 1D)

failed to assemble more than the proximal $(\alpha,\beta^*)_3G$ heterohexameric disc, in spite of the absence of a sizable recombinant fusion protein P, suggesting that minor modifications to the C-terminus of the CpcB subunit could bring about changes in the spatial arrangement of the PC discs so as to prevent the full elongation of the PC peripheral rods.

Mass spectrometric analysis of the selective affinity-purified complexes showed the occasional presence, in trace amounts, of other cyanobacterial compounds. Among those, FNR was noted in the eluted fractions. FNR catalyzes the electron transfer reaction between reduced ferredoxin and NADP+ and is reportedly localized at the proximal or distal PC disc of the PBS.[48−50] Such FNR adherence to PC may explain its elution along with the $(\alpha,\beta^*P)_3G$ heterohexameric disc from the affinity chromatography column. Additional PC linker polypeptides in trace/negligible amounts were occasionally detected in some of the transformants, for example, CpcC1 and CpcD, but these were not consistently present in the elution fractions and could be thought of as random contaminants.

In summary, evidence provided in this work showed that the CpcB*P fusion proteins, multiple examples of which have been shown to stably accumulate in cyanobacterial transformants, comprise an $(\alpha,\beta^*P)_3CpcG1$ heterohexameric fusion protein complex (Figure 11A), which assembles in a functional association with the AP core cylinders, absorbing sunlight and transferring excitation energy from the α,β PC subunits to the PSII reaction center (Figure 11B). In essence, the work showed that recombinant protein accumulation in fusion constructs is attained because of the cellular need to employ the recombinant constructs as a minimal PC antenna for its own use and benefit. The outwardly oriented heterologous proteins P in these $(\alpha,\beta^*P)_3G$ heterohexameric complexes are exposed to the soluble cytosol and evidently retain catalytic activity, when P is an enzyme rather than a structural protein, offering the possibility of catalysis for the synthesis of heterologous products.[19,20,31−36,40,41]

■ METHODS

Strains, Recombinant Constructs, Culture Conditions, and Fitness of the Transformants. The unicellular cyanobacterium *Synechocystis* sp. PCC 6803 (*Synechocystis*) WT strain was used as the reference strain for the experiments described in this work. Transformants *cpcB*6xHis*tev*IFN* (abbreviated as CpcB*IFN), *cpcB*6xHis*tev*TTFC* (CpcB*TTFC), and Δ*cpc* have been described in recent studies from this lab.[6,33,36] The generation of transformant *cpcB*6xHis*tev* (abbreviated as CpcB*) was achieved by the deletion of the TTFC sequence gene from the CpcB*TTFC construct using the Q5 site-directed mutagenesis kit (New England Biolabs) and by the use of primers Δ*ttfc_fw* (5′-TGAGGAATTAGGAGGTAATATATG-3′) and Δ*ttfc_rv* (5′-GCCTTGTAAATACAAATTATCATG-3′).

Transformation of *Synechocystis* was performed according to the protocols earlier described.[51−53] All strains were maintained on BG11 media supplemented with 1% agar, 10 mM triethylsilane (TES)−NaOH (pH 8.2), 0.3% sodium thiosulfate, and the corresponding antibiotic (20 mg L^{-1} chloramphenicol, 15 mg L^{-1} spectinomycin, or 10 mg L^{-1} kanamycin). Cell suspensions in liquid culture were cultivated in 1 L bottles, buffered with 37.5 mM sodium bicarbonate and 6.25 mM dipotassium hydrogen phosphate (pH 9), instead of TES buffer, and incubated in the light with continuous gentle agitation. Illumination was provided with a balanced combination of a

white light-emitting diode and incandescent light bulbs to yield a final photosynthetically active radiation intensity of ~100 μmol photons m^{-2} s^{-1}. Rates of growth of the transformants were conducted as described[35,36] to ensure that cell viability properties were not affected by the transformations performed in this work.

Genomic DNA PCR Analysis and Homoplasmy Testing. *Synechocystis* genomic DNA was extracted and prepared as described.[15] Briefly, 10 μL of cell suspension from a culture in the intermediate exponential growth phase (OD730 ~ 1) was mixed with 10 μL of 100% ethanol and, then, 100 μL of 10% (w/v) Chelex100 Resin (BioRad, Hercules, CA) was added. This mix was incubated at 98 °C for 10 min, followed by centrifugation at 16,000g for 10 min. Two and a half microliters of the supernatant were used as a template in a 12.5 μL PCR reaction. Q5 High-Fidelity 2X Master Mix (New England Biolabs, Ipswich, MA) was used to perform the analysis. The state of genomic DNA homoplasmy was tested after a few rounds of selection with the appropriate antibiotic. The primers used for this test were *cpcB_fw* (5′-TGACATGGAAAT-CATCCTCC-3′) and *cpcA_rv* (5′-GGTGGAAACGGCTT-CAGTTAAAG-3′). The location of these primers on the DNA constructs are indicated in Figure 1 with forward and reverse arrows for the respective DNA constructs.

Protein Extraction, Purification, and Electrophoresis. Fifty milliliters of cell suspension in the intermediate exponential growth phase (OD730 ~ 1) was pelleted by centrifugation at 4500g for 5 min. The cells were suspended in 2 mL of a solution buffered with 50 mM Tris-HCl, pH 8.2, supplemented with a cOmplete mini protease inhibitor cocktail (Roche), and kept on ice. Then, cells were broken by passing the suspension twice through a French press cell at 1500 psi. The unbroken cells were removed by centrifugation at a slow speed of 350g for 3 min. The supernatant with the crude cell extracts was kept on ice until use or at −80 °C for long-term storage.

Recombinant protein purification was performed using 400 μL of total crude cellular extracts mixed with 1 M HEPES-NaOH buffer, pH = 7.5, and Triton X-100 to yield final concentrations of 20 mM and 0.2%, respectively. This mix was incubated at room temperature for 20 min with gentle shaking. After this incubation, samples were centrifuged for 5 min at 16,000g to remove cell debris and insoluble material. The supernatant was mixed with 100 μL of HIS-Select cobalt affinity gel (Sigma-Aldrich, St. Louis, MO, United States) for the cobalt affinity chromatography. Selective elution of the fusion proteins was performed according to the manufacturer's recommendations.

Samples for denatured electrophoretic analysis of proteins (SDS-PAGE) were solubilized for 30 min at room temperature in the presence of 1× Laemmli sample buffer (BioRad, Hercules, CA), supplemented with a final concentration of 1 M urea and 5% β-mercaptoethanol. The samples were briefly vortexed every 10 min to enhance solubilization. Prior to loading onto SDS-PAGE, samples were centrifuged at 16,000g for 3 min to remove cell debris and insoluble material. Samples for native PAGE analysis were just mixed with equal parts of 2× loading buffer (62.5 mM Tris-HCl, pH 6.8, 40% glycerol, and 0.01% bromophenol blue) prior to loading the PAGE lanes. The SDS-PAGE and native PAGE were performed with a lane load of 20 μL, using the 12-well any kDa Mini-PROTEAN TGX precast protein gels. (BioRad, Hercules, CA). Densitometric analysis of protein bands was performed using BioRad (Hercules, CA) Image Lab software, measured from the scanning of the

Coomassie-stained gel lanes. Protein band ratios were measured from the scans of Coomassie-stained SDS-PAGE gels.

Zinc and Coomassie Staining. SDS-PAGE or native PAGE was performed in the presence of 5 mM zinc sulfate for 30 min.[33,54] To detect covalent chromophore-binding polypeptides, zinc-induced fluorescence was measured using the ChemiDoc imaging system (BioRad), employing UV irradiance as a light source. After registering the Zn-chromophore fluorescence, gels were incubated overnight in a solution of 0.1% Coomassie Blue G, 37% methanol, 3% phosphoric acid, and 17% ammonium sulfate. Finally, gels were washed with 5% acetic acid to remove excess Coomassie stain. Densitometric quantification of target proteins was performed using BioRad (Hercules, CA) Image Lab software.

Protein Analysis Using Mass Spectrometry. Mass spectrometry was performed at the Vincent J. Coates Proteomics/Mass Spectrometry Laboratory at UC Berkeley. Sample preparation was performed according to the internal protocols of the Vincent J. Coates Lab. In brief, digestion of proteins in SDS-PAGE slices consisted of washing the gel pieces for 20 min in 100 mM NH$_4$HCO$_3$. After discarding the first wash, an incubation at 50 °C with 100 mM NH$_4$HCO$_3$ and 45 mM DTT was performed for 15 min. To the cooled down mix, 100 mM iodoacetamide was added and incubated in the dark for 15 min. Then, the solvent was discarded, and the gel slice was washed with a 50:50 mix of acetonitrile and 100 mM NH$_4$HCO$_3$ with shaking for 20 min. The wash was repeated with only acetonitrile, followed by drying of the gel fragments in a SpeedVac. The gel pieces were rinsed thoroughly with 25 mM NH$_4$HCO$_3$ containing Promega-modified trypsin and incubated for 8 h at 37 °C. The supernatant was removed and placed in new microcentrifuge tubes. To extract the remaining peptides, the gel pieces were treated by adding 60% acetonitrile and 0.1% formic acid for 20 min and then once with acetonitrile. Finally, the supernatant was subjected to SpeedVac to dryness. Fusion proteins from the cobalt affinity chromatography and selective elution were buffer exchanged with 8 M urea and 100 mM Tris-HCl, pH 8.5, prior to been treated with the reducing, alkylating agent and the corresponding digestion steps mentioned above.

A nano liquid chromatography column was packed in a 100 μm inner diameter glass capillary with an emitter tip. The column consisted of 10 cm of Polaris c18 5 μm packing material. The column was loaded by use of a pressure bomb and washed extensively with buffer A solution (see below). The column was then directly coupled to an electrospray ionization source mounted on a Thermo Fisher LTQ XL linear ion trap mass spectrometer. An Agilent 1200 high-performance liquid chromatograph equipped with a split line so as to deliver a flow rate of 300 nL min^{-1} was used for chromatography. Peptides were eluted with a 90-minus gradient to 60% B. Buffer A contained 5% acetonitrile and 0.02% heptafluorobutyric acid (HFBA). Buffer B contained 80% acetonitrile and 0.02% HFBA.

Protein identification was performed with Integrated Proteomics Pipeline (IP2, Integrated Proteomics Applications, Inc. San Diego, CA) using ProLuCID/Sequest, DTASelect2, and Census.[55,56,58,57] Tandem mass spectra were extracted into ms1 and ms2 files from raw files using RawExtractor.[59] Data were searched against a database of *Synechocystis* sp. PCC6803 downloaded from Uniprot in December 2020 and supplemented with sequences of possible common contaminants. The database was concatenated to a decoy database in which the sequence for each entry in the original database was reversed.[60] LTQ data were searched with a 3000.0 milli-amu precursor

tolerance, and the fragment ions were restricted to a 600.0 ppm tolerance. All searches were parallelized and searched on the VJC proteomics cluster. The search space included all fully tryptic peptide candidates with no missed cleavage restrictions. Carbamidomethylation (+57.02146) of cysteine was considered a static modification. We required one peptide per protein and both tryptic termini for each peptide identification. The ProLuCID search results were assembled and filtered using the DTASelect program[56,58] with a peptide false discovery rate (FDR) of 0.001 for single peptide and a peptide FDR of 0.005 for additional peptides of the same protein.

In addition to the sequence coverage, the values of NSAF[61] and the emPAI[62] were calculated from the mass spectrometry analysis to help understand the amounts of the hits observed in the sample; in this context, the values of the NSAF showed that the abundance of the CpcG1 protein prevailed over the other hits after being normalized by the effect of the number of spectra counted. The emPAI indicates that the concentration of CpcG1 is approximately 3 times higher than that of CpcG2 and 25-fold greater at the last hit.

Photosystem II Absorption Cross-Section Measurements. Absorbance measurements of the WT and fusion construct mutants were obtained with cell suspensions in the growth medium. The absorbance spectra were recorded from 550 to 750 nm only to emphasize the relationship between the Chl and PC content of the cells (Figure 10). The flattening (attenuation) of the absorbance at 620 nm was estimated from the absorbance of the intact cells as compared to that of lysed samples in which the pigments were more uniformly distributed in the suspension, as earlier described.[63]

Rates of light absorption and the associated effective light-harvesting antenna size of photosystem-II in the various *Synechocystis* transformants were measured from the Chl fluorescence induction kinetics of cells suspended in the presence of 12 or 24 μM DCMU-treated cells, as previously described.[38,39] Weak actinic excitation (10 μmol photons m^{-2} s^{-1}) was defined at 619.5 nm by a narrow bandpass Baird Atomic interference filter coupled with a 659.6 nm visible bandpass negative cutoff Ealing filter. Chl fluorescence emission was recorded at 700 nm, defined by a 700 nm narrow bandpass Baird Atomic interference filter coupled with a 695 nm red cutoff Schott filter. The rate constant of light absorption by PSII was measured from the slope of the straight line, following a first-order kinetic analysis of the area accumulation over the variable fluorescence induction curve. The latter is a direct measure of the kinetics of Q_A photoreduction under these experimental conditions.[38,39]

ASSOCIATED CONTENT

Ⓢ Supporting Information

The Supporting Information is available free of charge at https://pubs.acs.org/doi/10.1021/acssynbio.1c00449.

> Sequence of oligonucleotide primers used in this work; density values of the Coomassie-stained protein bands; SDS-PAGE Zn-chromophore fluorescence analysis of eluted protein fractions from CpcB* (21 kDa), CpcB*IFN (36 kDa), and CpcB*TTFC (73 kDa); calibration and measurement of the CpcB*TTFC fusion complex molecular mass based on its relative electrophoretic mobility; DNA and protein Sequences used in this work; and DNA and amino acid sequences for the CpcB*IFN, CpcB*TTFC, and CpcB* constructs as well as for the *cpcG1* and *cpcG2* genes (PDF)

AUTHOR INFORMATION

Corresponding Author

Anastasios Melis − *Plant and Microbial Biology, University of California, Berkeley, California 94720-3102, United States;* ⓞ orcid.org/0000-0003-2581-4177; Email: melis@ berkeley.edu

Authors

Diego Hidalgo Martinez − *Plant and Microbial Biology, University of California, Berkeley, California 94720-3102, United States;* ⓞ orcid.org/0000-0002-8086-7469

Nico Betterle − *Plant and Microbial Biology, University of California, Berkeley, California 94720-3102, United States*

Complete contact information is available at:
https://pubs.acs.org/10.1021/acssynbio.1c00449

Author Contributions

D.H.M., N.B., and A.M. designed the project. D.H.M. and A.M. conducted the experimental work. D.H.M. drafted the figures and wrote the first version of the manuscript, which was edited by A.M. and N.B.

Notes

The authors declare no competing financial interest.

ABBREVIATIONS

AP, allophycocyanin; PC, phycocyanin; *cpcA*, gene encoding the PC α-subunit; *cpcB*, gene encoding the PC β-subunit; *cpcG*, gene encoding the proximal PC linker protein CpcG1/CpcG2; *Synechocystis*, Synechocystis sp. PCC 6803; PBS, phycobilisome; PSII, photosystem II; Chl, chlorophyll; WT, wild type

REFERENCES

(1) Grossman, A. R.; Bhaya, D.; Apt, K. E.; Kehoe, D. M. Light-harvesting complexes in oxygenic photosynthesis: Diversity, Control, and Evolution. *Annu. Rev. Genet.* **1995**, *29*, 231−288.

(2) Yamanaka, G.; Glazer, A. N.; Williams, R. C. Cyanobacterial phycobilisomes. Characterization of the phycobilisomes of *Synechococcus* sp. 6301. *J. Biol. Chem.* **1978**, *253*, 8303−8310.

(3) Yamanaka, G.; Lundell, D. J.; Glazer, A. N. Molecular architecture of a light-harvesting antenna. Isolation and characterization of phycobilisome subassembly particles. *J. Biol. Chem.* **1982**, *257*, 4077−4086.

(4) Ughy, B.; Ajlani, G. Phycobilisome rod mutants in *Synechocystis* sp. strain PCC 6803. *Microbiology* **2004**, *150*, 4147−4156.

(5) Watanabe, M.; Ikeuchi, M. Phycobilisome: architecture of a light-harvesting supercomplex. *Photosynth. Res.* **2013**, *116*, 265−276.

(6) Kirst, H.; Formighieri, C.; Melis, A. Maximizing photosynthetic efficiency and culture productivity in cyanobacteria upon minimizing the phycobilisome light-harvesting antenna size. *Biochim. Biophys. Acta, Bioenerg.* **2014**, *1837*, 1653−1664.

(7) Sidler, W. A. Phycobilisome and phycobiliprotein structures. *The Molecular Biology of Cyanobacteria*; Bryant, D. A., Ed.; Advances in Photosynthesis; Springer: Dordrecht, 1994; Vol. *1*.

(8) Liu, L.-N.; Chen, X.-L.; Zhang, Y.-Z.; Zhou, B.-C. Characterization, structure and function of linker polypeptides in phycobilisomes of cyanobacteria and red algae: An overview. *Biochim. Biophys. Acta* **2005**, *1708*, 133−142.

(9) Elmorjani, K.; Herdman, M. Metabolic control of phycocyanin degradation in the cyanobacterium *Synechocystis* pcc 6803: a glucose effect. *J. Gen. Microbiol.* **1987**, *133*, 1685−1694.

(10) Collier, J. L.; Grossman, A. R A small polypeptide triggers complete degradation of light-harvesting phycobiliproteins in nutrient-deprived cyanobacteria. *EMBO J.* **1994**, *13*, 1039−1047.

(11) Richaud, C.; Zabulon, G.; Joder, A.; Thomas, J.-C. Nitrogen or sulfur starvation differentially affects phycobilisome degradation and expression of the *nbla* gene in *Synechocystis* strain PCC 6803. *J. Bacteriol.* **2001**, *183*, 2989−2994.

(12) De Marsac, N. T.; Cohen-Bazire, G. Molecular composition of cyanobacterial phycobilisomes. *Proc. Natl. Acad. Sci. U.S.A.* **1977**, *74*, 1635−1639.

(13) Kondo, K.; Geng, X. X.; Katayama, M.; Ikeuchi, M. Distinct roles of CpcG1 and CpcG2 in phycobilisome assembly in the cyanobacterium *Synechocystis* sp. PCC 6803. *Photosynth. Res.* **2005**, *84*, 269−273.

(14) Bolte, K.; Kawach, O.; Prechtl, J.; Gruenheit, N.; Nyalwidhe, J.; Maier, U. G. Complementation of a phycocyanin-bilin lyase from *Synechocystis* sp. PCC 6803 with a nucleomorph-encoded open reading frame from the cryptophyte Guillardia theta. *BMC Plant Biol.* **2008**, *8*, 56.

(15) Formighieri, C.; Melis, A. Regulation of β-phellandrene synthase gene expression, recombinant protein accumulation, and monoterpene hydrocarbons production in *Synechocystis* transformants. *Planta* **2014**, *240*, 309−324.

(16) Zhou, J.; Zhang, H.; Meng, H.; Zhu, Y.; Bao, G.; Zhang, Y.; Li, Y.; Ma, Y. Discovery of a super-strong promoter enables efficient production of heterologous proteins in cyanobacteria. *Sci. Rep.* **2014**, *4*, 4500.

(17) Davies, F. K.; Work, V. H.; Beliaev, A. S.; Posewitz, M. C. Engineering limonene and bisabolene production in wild type and a glycogen-deficient mutant of *Synechococcus* sp. PCC 7002. *Front. Bioeng. Biotechnol.* **2014**, *2*, 21.

(18) Englund, E.; Liang, F.; Lindberg, P. Evaluation of promoters and ribosome binding sites for biotechnological applications in the unicellular cyanobacterium *Synechocystis* sp. PCC 6803. *Sci. Rep.* **2016**, *6*, 36640.

(19) Betterle, N.; Melis, A. Photosynthetic generation of heterologous terpenoids in cyanobacteria. *Biotechnol. Bioeng.* **2019**, *116*, 2041−2051.

(20) Betterle, N.; Melis, A. Heterologous leader sequences in fusion constructs enhance expression of geranyl diphosphate synthase and yield of β-phellandrene production in cyanobacteria (*Synech..ocystis*). *ACS Synth. Biol.* **2018**, *7*, 912−921.

(21) Lim, H.; Park, J.; Woo, H. M. Overexpression of the key enzymes in the methylerythritol 4-phosphate pathway in *Corynebacterium glutamicum* for improving farnesyl diphosphate-derived terpene production. *J. Agric. Food Chem.* **2020**, *68*, 10780−10786.

(22) Demain, A. L.; Vaishnav, P. Production of recombinant proteins by microbes and higher organisms. *Biotechnol. Adv.* **2009**, *27*, 297−306.

(23) Surzycki, R.; Greenham, K.; Kitayama, K.; Dibal, F.; Wagner, R.; Rochaix, J.-D.; et al. Factors effecting expression of vaccines in microalgae. *Biologicals* **2009**, *37*, 133−138.

(24) Tran, M.; Zhou, B.; Pettersson, P. L.; Gonzalez, M. J.; Mayfield, S. P. Synthesis and assembly of a full-length human monoclonal antibody in algal chloroplasts. *Biotechnol. Bioeng.* **2009**, *104*, a−n.

(25) Coragliotti, A. T.; Beligni, M. V.; Franklin, S. E.; Mayfield, S. P. Molecular factors affecting the accumulation of recombinant proteins in the Chlamydomonas reinhardtii chloroplast. *Mol. Biotechnol.* **2011**, *48*, 60−75.

(26) Gregory, J. A.; Topol, A. B.; Doerner, D. Z.; Mayfield, S. Alga-produced cholera toxin-Pfs25 fusion proteins as oral vaccines. *Appl. Environ. Microbiol.* **2013**, *79*, 3917−3925.

(27) Jones, C. S.; Mayfield, S. P. Steps toward a globally available malaria vaccine: harnessing the potential of algae for future low-cost vaccines. *Bioengineered* **2013**, *4*, 164−167.

(28) Rasala, B. A.; Mayfield, S. P. Photosynthetic biomanufacturing in green algae; production of recombinant proteins for industrial, nutritional, and medical uses. *Photosynth. Res.* **2015**, *123*, 227−239.

(29) Baier, T.; Kros, D.; Feiner, R. C.; Lauersen, K. J.; Müller, K. M.; Kruse, O. Engineered fusion proteins for efficient protein secretion and purification of a human growth factor from the green microalga *Chlamydomonas reinhardtii*. *ACS Synth. Biol.* **2018**, *7*, 2547−2557.

(30) Dyo, Y. M.; Purton, S. The algal chloroplast as a synthetic biology platform for production of therapeutic proteins. *Microbiology* **2018**, *164*, 113−121.

(31) Formighieri, C.; Melis, A. A phycocyanin●phellandrene synthase fusion enhances recombinant protein expression and β-phellandrene (monoterpene) hydrocarbons production in *Synechocystis* (cyanobacteria). *Metab. Eng.* **2015**, *32*, 116−124.

(32) Chaves, J. E.; Rueda-Romero, P.; Kirst, H.; Melis, A. Engineering isoprene synthase expression and activity in cyanobacteria. *ACS Synth. Biol.* **2017**, *6*, 2281−2292.

(33) Betterle, N.; Hidalgo Martinez, D.; Melis, A. Cyanobacterial production of biopharmaceutical and biotherapeutic proteins. *Front. Plant Sci.* **2020**, *11*, 237.

(34) Chaves, J. E.; Romero, P. R.; Kirst, H.; Melis, A. Role of isopentenyl-diphosphate isomerase in heterologous cyanobacterial (*Synechocystis*) isoprene production. *Photosynth. Res.* **2016**, *130*, 517−527.

(35) Chaves, J. E.; Melis, A. Biotechnology of cyanobacterial isoprene production. *Appl. Microbiol. Biotechnol.* **2018**, *102*, 6451−6458.

(36) Zhang, X.; Betterle, N.; Hidalgo Martinez, D.; Melis, A. Recombinant protein stability in cyanobacteria. *ACS Synth. Biol.* **2021**, *10*, 810−825.

(37) Duyens, L. N. M. The flattening of the absorption spectrum of suspensions, as compared to that of solutions. *Biochim. Biophys. Acta* **1956**, *19*, 1−12.

(38) Melis, A.; Duysens, L. N. M. Biphasic energy conversion kinetics and absorbance difference spectra of photosystem II of chloroplasts. Evidence for two different system II reaction centers. *Photochem. Photobiol.* **1979**, *29*, 373−382.

(39) Melis, A. Spectroscopic methods in photosynthesis: photosystem stoichiometry and chlorophyll antenna size. *Philos. Trans. R. Soc. London, Ser. B* **1989**, *323*, 397−409.

(40) Formighieri, C.; Melis, A. Cyanobacterial production of plant essential oils. *Planta* **2018**, *248*, 933−946.

(41) Formighieri, C.; Melis, A. Heterologous synthesis of geranyllinalool, a diterpenol plant product, in the cyanobacterium. *Synechocystis*. *Appl. Microbiol. Biotechnol.* **2017**, *101*, 2791−2800.

(42) David, L.; Marx, A.; Adir, N. High-resolution crystal structures of trimeric and rod phycocyanin. *J. Mol. Biol.* **2011**, *405*, 201−213.

(43) Kondo, K.; Mullineaux, C. W.; Ikeuchi, M. Distinct roles of CpcG1-phycobilisome and CpcG2-phycobilisome in state transitions in a cyanobacterium *Synechocystis* sp. PCC 6803. *Photosynth. Res.* **20092009**, *99*, 217−225.

(44) Kondo, K.; Ochiai, Y.; Katayama, M.; Ikeuchi, M. The Membrane-associated CpcG2-phycobilisome in *Synechocystis*: A new photosystem I antenna. *Plant Physiol.* **2007**, *144*, 1200−1210.

(45) Baier, A.; Winkler, W.; Korte, T.; Lockau, W.; Karradt, A. Degradation of phycobilisomes in *Synechocystis* sp. pcc6803 evidence for essential formation of an nbla1/nbla2 heterodimer and its codegradation by a clp protease complex. *J. Biol. Chem.* **2014**, *289*, 11755−11766.

(46) Chang, L.; Liu, X.; Li, Y.; Liu, C.-C.; Yang, F.; Zhao, J.; et al. Structural organization of an intact phycobilisome and its association with photosystem II. *Cell Res.* **2015**, *25*, 726−737.

(47) Guan, X.; Qin, S.; Zhao, F.; Zhang, X.; Tang, X. Phycobilisomes linker family in cyanobacterial genomes: divergence and evolution. *Int. J. Biol. Sci.* **2007**, *3*, 434−445.

(48) Arteni, A. A.; Ajlani, G.; Boekema, E. J. Structural organisation of phycobilisomes from *Synechocystis* sp. strain PCC6803 and their interaction with the membrane. *Biochim. Biophys. Acta, Bioenerg.* **2009**, *1787*, 272−279 A:.

(49) Gómez-Lojero, C.; Pérez-Gómez, B.; Shen, G.; Schluchter, W. M.; Bryant, D. A. Interaction of ferredoxin:NADP⁺ oxidoreductase with phycobilisomes and phycobilisome substructures of the cyanobacte-

rium *Synechococcus* sp. strain PCC 7002. *Biochemistry* **2003**, *42*, 13800−13811.

(50) Van Thor, J. J.; Gruters, O. W. M.; Matthijs, H. C. P.; Hellingwerf, K. J. Localization and function of ferredoxin:NADP⁺ reductase bound to the phycobilisomes of *Synechocystis*. *EMBO J.* **1999**, *18*, 4128−4136.

(51) Williams, J. G. K. Construction of specific mutations in Photosystem II photosynthetic reaction center by genetic engineering methods in *Synechocystis* 6803. *Methods Enzymol.* **1988**, *167*, 766−778.

(52) Eaton-Rye, J. J. Construction of gene interruptions and gene deletions in the cyanobacterium *Synechocystis* sp. Strain PCC 6803. In *Photosynthesis Research Protocols*; Carpentier, R., Ed.; Methods in Molecular Biology (Methods and Protocols); Humana Press: Totowa, 2011; Vol. *684684*. http://link.springer.com/10.1007/978-1-60761-925-3.

(53) Lindberg, P.; Park, S.; Melis, A. Engineering a platform for photosynthetic isoprene production in cyanobacteria, using *Synechocystis* as the model organism. *Metab. Eng.* **2010**, *12*, 70−79.

(54) Li, Y.; Lin, Y.; Garvey, C. J.; Birch, D.; Corkery, R. W.; Loughlin, P. C.; Scheer, H.; Willows, R. D.; Chen, M. Characterization of red-shifted phycobilisomes isolated from the chlorophyll *f*-containing cyanobacterium *Halomicronema hongdechloris*. *Biochim. Biophys. Acta* **2016**, *1857*, 107−114.

(55) Xu, T.; et al. ProLuCID, a fast and sensitive tandem mass spectra-based protein identification program. *Mol. Cell. Proteomics* **2006**, *5*, S174.

(56) Cociorva, D.; Yates, J. R.; Validation of tandem mass spectrometry database search results using DTASelect. *Current Protocols in Bioinformatics*; Baxevanis, A. D., et al.; Wiley, 2007; Chapter 13: Unit 13.4.

(57) Park, S. K.; Venable, J. D.; et al. A quantitative analysis software tool for mass spectrometry-based proteomics. *Nat. Methods* **2008**, *5*, 319−322.

(58) Tabb, D. L.; McDonald, W. H.; Yates, J. R., III DTASelect and Contrast: tools for assembling and comparing protein identifications from shotgun proteomics. *J. Proteome Res.* **2002**, *1*, 21−26.
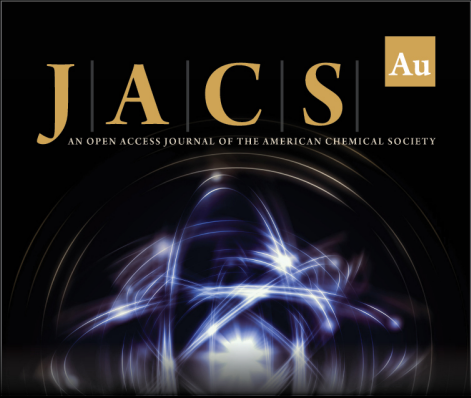
(59) McDonald, W. H.; Tabb, D. L.; Sadygov, R. G.; MacCoss, M. J.; Venable, J.; et al. MS1, MS2, and SQT-three unified, compact, and easily parsed file formats for the storage of shotgun proteomic spectra and identifications. *Rapid Commun. Mass Spectrom.* **2004**, *18*, 2162−2168.

(60) Peng, J.; Elias, J. E.; Thoreen, C. C.; Licklider, L. J.; Gygi, S. P. Evaluation of multidi-mensional chromatography coupled with tandem mass spectrometry (LC/LC-MS/MS) for large-scale protein analysis: the yeast proteome. *J. Proteome Res.* **2003**, *2*, 43−50.

(61) Zybailov, B.; Mosley, A. L.; Sardiu, M. E.; Coleman, M. K.; Florens, L.; Washburn, M. P. Statistical analysis of membrane proteome expression changes in *Saccharomyces cerevisiae*. *J. Proteome Res.* **2006**, *5*, 2339−2347.

(62) Ishihama, Y.; Oda, Y.; Tabata, T.; Sato, T.; Nagasu, T.; Rappsilber, J.; et al. Exponentially modified protein abundance index (emPAI) for estimation of absolute protein amount in proteomics by the number of sequenced peptides per protein. *Mol. Cell. Proteomics* **2005**, *4*, 1265−1272 [Internet].

(63) Pulles, M. P. J.; Van Gorkom, H. J.; Verschoor, G. A. M. Primary reactions of photosystem II at low pH. 2. Light-induced changes of absorbance and electron spin resonance in spinach chloroplasts. *Biochim. Biophys. Acta* **1976**, *440*, 98−106.

O